Journal of Power Sources 196 (2011) 6588–6594

Contents lists available at ScienceDirect

Journal of Power Sources

journal homepage: www.elsevier.com/locate/jpowsour

Comprehensive thermal modeling of a power-split hybrid powertrain using battery cell model

Abdel Raouf Mayyas[a], Mohammed Omar[a,*], Pierluigi Pisu[a], Ali Al-Ahmer[b], Ahmad Mayyas[a], Carlos Montes[b], Shan Dongri[a,c]

[a] Automotive Engineering Department, Clemson University International Center for Automotive Research CU-ICAR, 4 Research Drive Greenville 29607, United States
[b] Mechanical Engineering Department, Clemson University, Clemson SC 29634, United States
[c] School of Mechanical Engineering, Shandong Institute, China

ARTICLE INFO

Article history:
Received 16 February 2011
Received in revised form 15 March 2011
Accepted 15 March 2011
Available online 24 March 2011

Keywords:
Finite differencing
Power-split hybrid architecture
Cell based model
Thermal management
Driving cycles
Hybrid powertrain

ABSTRACT

This manuscript discusses the development of a 3D thermal model for a power-split hybrid powertrain, including its battery modules and power electronics. The 3D model utilizes a finite differencing (FD) heat transfer algorithm, complemented with experimental boundary conditions. The experimental setup is configured to acquire the battery current, voltage, and its inner and surface temperatures in discrete and in full-field scans. The power-split hybrid configuration is tested using a standard and artificial driving cycles. A battery resistance model is then used to couple the experimental boundary conditions with the finite differencing code, which employed a cell-based internal heat generation model to describe the pack chemical reaction mechanism. This study presents a complete analysis based on battery current and voltage in relation to vehicle speed. The proposed model also predicts the powertrain spatial and temporal temperature profiles in agreement with the vehicle actual conditions as indicated by the On-Board Diagnosis (OBD) module.

Published by Elsevier B.V.

1. Introduction

Hybrid electric vehicle "HEV" with its unique key characteristics (i.e. mechanical complexity, multiple driving modes, and multiple prime movers) as shown in Fig. 1, affects the existing vehicular thermal management systems. This effect results in new thermal issues that should be accounted for in order to enhance the overall vehicle performance and its different systems.

Thermal management is vital for both conventional (internal combustion engine propelled) and hybrid electric vehicles, because it decides on the vehicle's overall performance. Typically, thermal modeling is used in analyzing the thermal loads when applied to the under-hood components [1]; however, enhanced thermal packaging and optimized utilization strategies of as-built automotive parts require an advanced thermal management system and predictive tools. Such systems will aid in not only reducing the exhaust emissions but also it will result in weight and cost savings through devising new control strategies and optimized cooling systems. At the same time, ensuring a high-quality thermal management scheme for HEVs' is still a challenge due to following issues: firstly, the hybrid power-trains (battery) are still an add-on to the current vehicles' architecture and still suffer from a variety of unresolved thermal packaging issues. Secondly, additional challenges are imposed by the new thermal loads imposed on the electric parts, the electronics, and the energy storage system that have temperature dependant performance [3]. Additionally, current thermal modeling schemes cannot be scaled or extended readily to include hybrid power-trains because of the battery pack inclusion which has unique transient behavior caused by the charging and discharging modes and the additional complexity of the cooling system and packaging constraints.

Current vehicle thermal models focus on the under-hood components analyses. Fluent Inc. introduced a Computational Fluid Dynamics (CFD) tool for the under-hood components [2,3] that is aimed at enhancing the under-hood packaging design to optimize the heat removal and the management process. This model utilizes a dual-cell heat exchanger scheme to simulate the heat rejection non-uniformities at different ambient temperatures, assuming a uniform temperature at the exhaust manifold surface, with the exhaust pipes acting as the heat source. Also, this scheme employed a tetra-mesh which resulted in non-uniform elements' local heat conduction that further leads to inaccuracies in the model's predictions.

Priya in [4] presented a thermal model of as-built automotive parts using a software package (commercial name MuSES), assessed with thermography to extract the needed boundary condi-

* Corresponding author. Tel.: +1 864 283 7226; fax: +1 864 283 7208.
E-mail address: momar@clemson.edu (M. Omar).

0378-7753/$ – see front matter. Published by Elsevier B.V.
doi:10.1016/j.jpowsour.2011.03.036

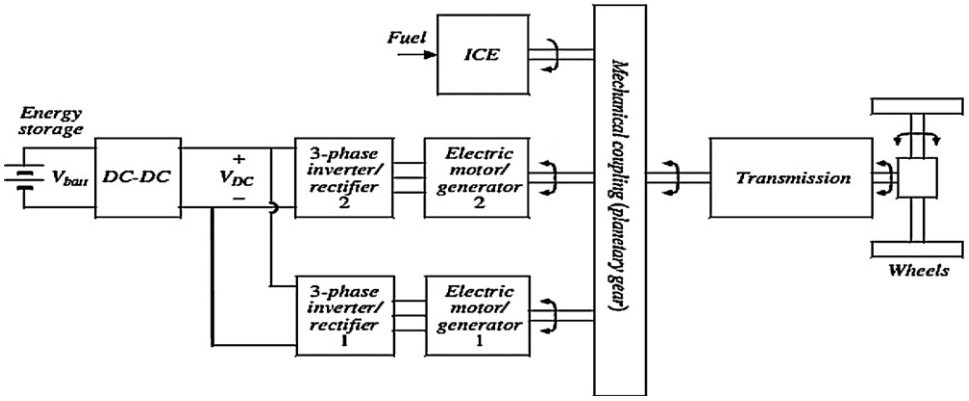

Fig. 1. Series/parallel HEVs' power train configuration [1].

tions. However this effort focused only on the engine compartment under idling conditions while targeting the exhaust manifold temperature fields.

Andreas et al. [5] discussed the use of a reverse geometry approach using thermal imaging to acquire the parts' topology, followed by modeling of the exhaust pipes using a finite element (FE) model. However, the acquired thermal geometries do not represent the actual surface 3D topographies but reconstructed fabrics from the thermal maps, which need to be further corrected to account for the surface view factors and its emissivities. Additionally, the thermal scans transient behavior was not captured; leading to loss of the lateral heat transfer through conduction. Furthermore, this approach cannot be applied to HEV's thermal management studies due to the variety of the added sub-systems and modules, which include the auxiliary re-generative braking system, the inverter, and the battery packs and its dedicated cooling.

In more related HEV research thermal management, Pesaran et al. [6] at the National Renewable Energy Laboratory (NREL) investigated the issues of integrating the battery cells into the packs for HEV's and Plug-In HEV's (PHEV's) to analyze its thermal performance. Pesaran in [7] introduced a lumped capacitance battery thermal model using advanced vehicle simulator (ADVISOR). The model considered the battery core and the battery casing as two separated iso-thermal nodes; however, all other components inside the battery-pack case were assumed to be a single homogeneous material with averaged properties. The heat generated inside the battery Q_{ess} (as evaluated by Ohm's law, i.e. $I^2 \times R$) is to be rejected to the ambient air through the casing via conduction and convection, and can be described mathematically as

$$Q_{ess\_case} = \frac{T_{ess} - T_{air}}{R_{eff}} \tag{1}$$

where T_{ess} is battery temperature (case or core), T_{air} is the air temperature, R_{eff} is a function of the conduction resistance through the case and the heat transfer film coefficient h on the air side, which is defined by

$$R_{eff} = \frac{1}{hA} + \frac{l}{kA} \tag{2}$$

where R_{eff} is the effective thermal resistance, h is the convective heat transfer film coefficient, k is the thermal conductivity coefficient, l and A are battery pack related parametric values. Whereas the convective heat transfer coefficient is a function of the parametric dimensions of the packs and the air flow properties as in the following

$$h = \begin{cases} h_{forced} = a\left(\dfrac{m/\rho A}{5}\right)^b \\ h_{natl} = 4 \end{cases} \tag{3}$$

with h_{forced} being the forced convective heat transfer coefficient, while a and b are battery packs' geometry related constants, and ρ is air density, see Ref. [7] for more details on how the packs' heat transfer coefficient is estimated.

The model estimated the packs temperature assuming that 50% of the heat from the battery goes into warming the air, hence it can be predicted by calculating the exit air temperature using (4)

$$T_{air} = T_{amb} + \frac{0.5 Q_{ess_case}}{\dot{m}_{air} C_{p,air}} dt \tag{4}$$

where $\dot{m}_{air}$ is air mass flow rate, and $C_{p,air}$ is the heat capacity of the air. Consequently, the temperature rise in the battery packs can then be calculated based on an energy balance as given by between battery heat generation (Q_{ess_gen}), amount of heat lost from the battery Q_{ess_case}, thermal mass of the battery ($m_{ess}\, C_{p,ess}$) and the duration of battery use (t) as shown in Eq. (5)

$$T_{ess} = \int_0^t \frac{Q_{ess\_gen} - Q_{ess\_case}}{m_{ess} C_{p,ess}} dt \tag{5}$$

2. Materials and methods

This section presents the basic steps and tools used to develop the model and to acquire the boundary conditions from an HEV system, running under standard and artificial driving cycles. The experimental work acquires the transient voltage, current, state of charge and temperature maps (discrete and full-field) for the HEV's Nickel Metal Hydrides NiMH battery packs in real-time.

Due to the differences between the series and the parallel HEV's powertrain layouts, a power-split hybrid configuration is used for testing; therefore, a 2010, third generation Toyota Prius is used, which is powered with a 52 kW Gasoline engine with a 34 kW electric motor, also the Prius III is equipped with a 201.6 V, 6.5 Ah, 36 HP NiMH battery pack, in addition to a synchronous electric motor with 80 HP/60 kW power output. The tested Panasonic NiMH Prius battery pack consists of 14 blocks with each block made of 12 prismatic cells to form a 6 module pack [8].

2.1. Experimental procedures

The Prius hybrid electric powertrain thermal performance is monitored under different transient power demands at the wheels with different speed profiles.

The standard drive cycle tests have demonstrated better predictions of battery life cycle and its performance, than the case with constant-current or constant-power cycling tests [9]. Therefore,

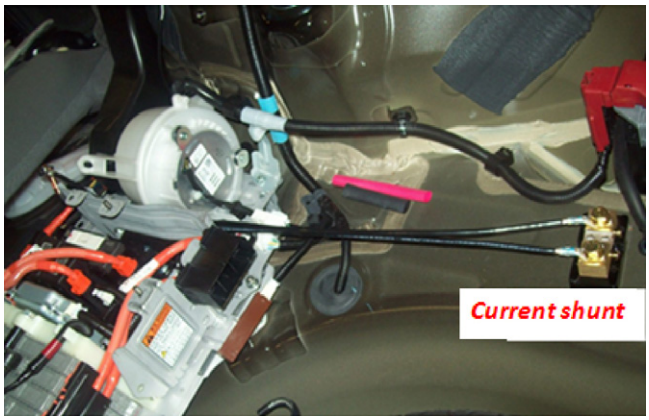

Fig. 2. Hardware set up for the current shunt circuitry.

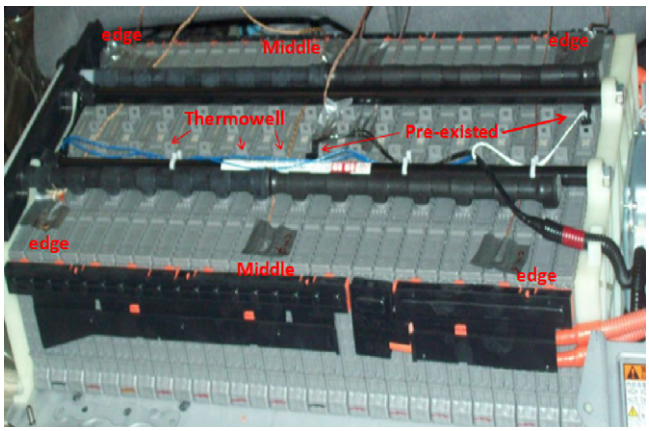

Fig. 3. Prius battery pack: OEM thermocouple, added thermocouples and thermowell.

Federal Urban Driving Schedule (FUDS), Federal Highway Driving Schedule (FHDS) in addition to an Artificial Driving Cycle (ADC) are employed to subject the HEV to different loading schemes. The ADC is used to help investigate the steady state behavior of the battery packs, which is considered necessary to establish and to calibrate the FD model [10,11]. Hence the ADC scheme is designed so that the vehicle is driven at a constant cruising speed for a 30 min trip while being divided into three intervals, whereas the speed increment is 15 mph every 10 min while starting at 30 mph and ending up at 60 mph.

A Renk Labeco 4-Wheel 500 HP chassis dynamometer is used to test the Prius under different road loads (i.e. vehicle speed). A driver-aid interface is developed to enable the operator to control the vehicle speed according to the predefined velocity profile using a compact Reconfigurable Input/Output platform (cRIO, product of National Instrument NI). The cRIO acquires the real time rollers' speed signal from the chassis dyno (0–10 V), translating it using LabView (NI-LV) [12].

2.2. Voltage, current, state of charge (SOC) data measurements

The battery pack current and voltage is acquired for each of the loading profiles. The electric current is measured using a current shunt circuitry, which acquires the voltage drop across a low Ohmic value resistor. The shunt is connected in series with negative terminals of the packs as in Fig. 2. The 200 A current shunt produces a 50 mV signal, which is then used by the 18 channels data acquisition system (commercial name eDAQ) to measure the voltage across the shunt resistor with a sampling rate of 100 Hz.

Because the state of charge (SOC) or the remaining capacity of the battery is dependent on the actual voltage level and the temperature; the On-Board Diagnosis (OBD) module is employed to record the transient measurements for the remaining capacity of the battery. At the same time, the OBD provides battery pack core temperature from three shielded thermocouples installed in three different positions (center, front and back) of the pack. Fig. 3 displays these positions along with the thermocouple network installed to trace the temperature variation within the pack.

2.3. Temperature measurements

The spatial and the temporal temperature profiles for the NiMH battery pack are also recorded for the different driving cycles using a thermal imager.

An un-cooled micro-bolometric infrared detector (commercial name Flir A40M, product of FLIR) calibrated for emissivity [13,14] is used to capture the pack 2D surface temperatures in real-time. The detector has a spatial resolution of 1.3 mrad, spectral range of 7.5–13 μm and a thermal sensitivity of 0.08 °C at 30 °C; it is capable of detecting temperature range of −40 to 500 °C with accuracy of 2% or 2 °C. Additionally, a thermocouple network is installed at different locations within the pack to provide a reference signal to correct and calibrate the infrared detector. The thermocouple network is connected to a high speed 8-channel Thermo Couple Interface Card (TCIC) with a sample rate of 10 Hz.

The same procedures are used to simultaneously capture the spatial temperature profiles for the engine, the exhaust manifold, the catalytic converter and the muffler. Meanwhile the thermocouples are used to obtain discrete temperature measurements for the engine's coolant and the hybrid system coolant temperature.

3. Test conditions

The on-board HEV tests started with the battery pack kept at room temperature around 22 °C, the FHDS cycle is applied, followed by a FUDS cycle, and then the ADC is lastly implemented. This mix of the different drive patterns helps to subject the battery pack to various modes of loading, i.e. charge/discharge cyclic load [19,20]. Additionally, the combination of both standard and artificial drive cycles will force the battery pack to experience both transient and steady-state loading schemes [21,22]. The FUDS reflects the city drive mode with frequent stop and go, while the FHDS represents the highway cruising, whereas the ADC reflects the long intervals of the steady-state power demands. It is important to mention that the battery pack is allowed to cool down close to the room temperature after each run using a forced air draft.

4. 3D model design

Finite Differencing (FD) code (commercial name RadTherm, product of Thermo-analytics) is used for the thermal modeling and analyses [23–25]; it includes an optimized thermal solver and it provides a 3D modeling with an image viewer (wireframe and animated thermal displays). A FD scheme is used due to its main advantages in solving models with non-uniform 3D curvilinear mesh; in addition FD is the most widely used discretizing technique for heat transfer problems; while finite element (FE) approach is more suited for fracture mechanics numerical simulation. The constructed model assigns the properties for each of the geometries to elements or group of elements that have the same thermal properties such as thickness, surface properties, imposed heat rates, heat rate versus time curves. Following the properties assignment, the solver discretizes the elements into thermal nodes. Also the net radiation exchange between any two surfaces which are assigned

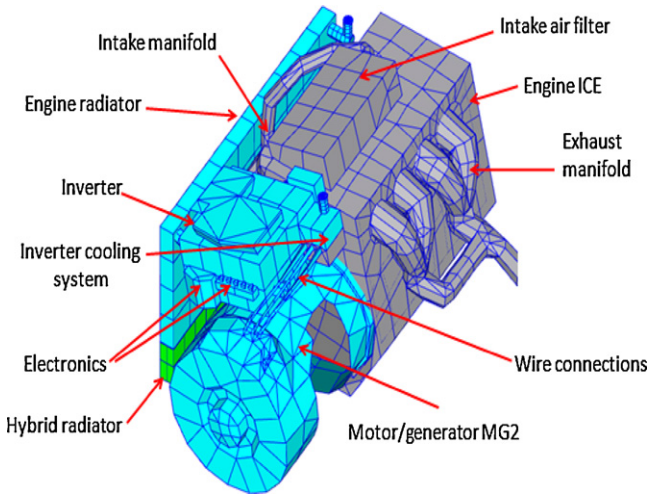

Fig. 4. "3D" FEM for hybrid electric power train for Prius.

to different thermal nodes i and j is calculated using Eq. (6) [24–26]

$$Q_{ij} = B_{ij}A_i\varepsilon_i\sigma_i(T_i^4 - T_j^4) \quad (6)$$

where Q is net radiation heat exchange in Watt, B_{ij} is the fraction of energy that is emitted from surface i and absorbed at surface j both directly and by reflection, A is area in m^2, ε is emissivity, σ is the Stefan–Boltzmann constant in $W\,m^2\,K^{-4}$, while T is the temperature of the objects (i and j) in Kelvin.

Subsequently, the solver calculates the viewing factors by iteratively rendering the objects' geometry as it is viewed by other surfaces linked to other thermal nodes. The solver computes the view factors in a single plane using the hemi-cube method. Moreover, the multi-layer of materials is represented by a grid of nodes defined within the same layer. One of the main advantages of the current solver, is its ability to establish thermal nodes while simulating the fluid streams. Although the model is set to calculate the nodes temperature based on an implicit technique, the explicit calculation can be done through an energy balance or by calculating the net energy rate (i.e. heat stored in the thermal node) as described in Eq. (7) [25].

$$\sum Q^* = mC_p\left(\frac{dT}{dt}\right) \quad (7)$$

where Q^* is the heat rate terms (Joules) including radiation and any imposed heat sources added by the analyst, m is the mass in kg, C_p is the specific heat $J\,(kg\,K)^{-1}$, and T is the temperature (K). Fig. 4 illustrates the 3D FE model for the Prius underhood hybrid electric powertrain modules.

Material properties, surface conditions, initial temperature were specified for each part. Fluid streams for engine coolant, exhaust gas, intake air, fuel, engine oil, hybrid system coolant, battery pack cooling air were also set up and bounded with its connected geometrical parts. Fluid nodes were created to link the fluid stream convection heat transfer to the back side of the bounding parts, where the thermal nodes were biased towards the center of the geometrical part. Fig. 5 illustrates the exhaust gas downstream bounded by the exhaust components (i.e. exhaust manifold ports, catalytic converter, muffler, and the exhaust pipes).

To provide an example of the fluid-stream settings, the exhaust gas fluid is linked to the back side of the engine cylinder-block, to simulate the air upstream which feeds the exhaust gas fluid downstream. Similarly, another fluid node is created to link the air inside the cabin to the back side of the passenger compartment, in order to simulate the air upstream that feeds the battery pack cooling air.

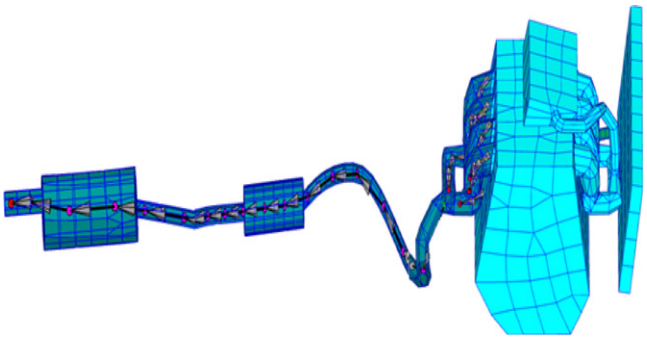

Fig. 5. Exhaust gas downstream bounded by the exhaust components.

Fundamental heat transfer and thermodynamic Otto cycle equations are employed to predict the exhaust gas temperature inside the cylinder, while the OBD provided the necessary data required for such task (flow rates, rpm, etc.), hence the heat generated during the combustion process can be calculated in Eq. (8);

$$m_f c_v(\Delta T) = m_f Q_{HV} \quad (8)$$

where m_f is mass of the fuel, C_v is the specific heat of the fuel at constant volume, Q_{HV} is the fuel heating value.

In regard to the battery pack, the battery cell FE model is designed with a high resolution (i.e. fine mesh) with the air cooling fluid streams created according to the designed schemes available from the Original Equipment Manufacturer (OEM). The cooling fan modes determine the corresponding cooling air mass flow rate, with the inhaling air conditions coupled with the compartment environment.

Additionally, a fluid node is created and linked to the back side of every cell in the (168 cells) pack, to simulate the fluid (i.e. the electrolyte) inside the battery cell, a temperature curve obtained from the three pre-existed thermo couples mentioned previously is also assigned to a fluid node inside each battery cell. Fig. 6 illustrates the battery pack air cooling fluid streams. Additional fluid nodes are created to link the model front side with ambient air, in a way to

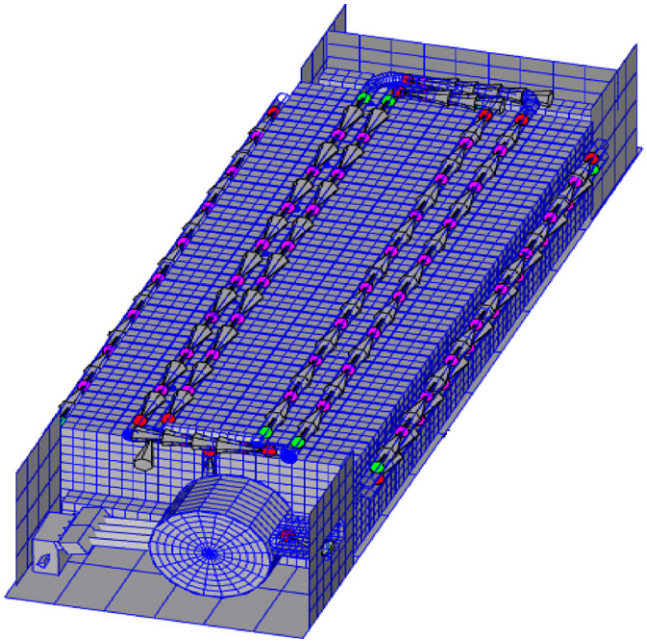

Fig. 6. Illustrates the battery pack air cooling fluid streams bounded by the cooling pipes surrounding the pack.

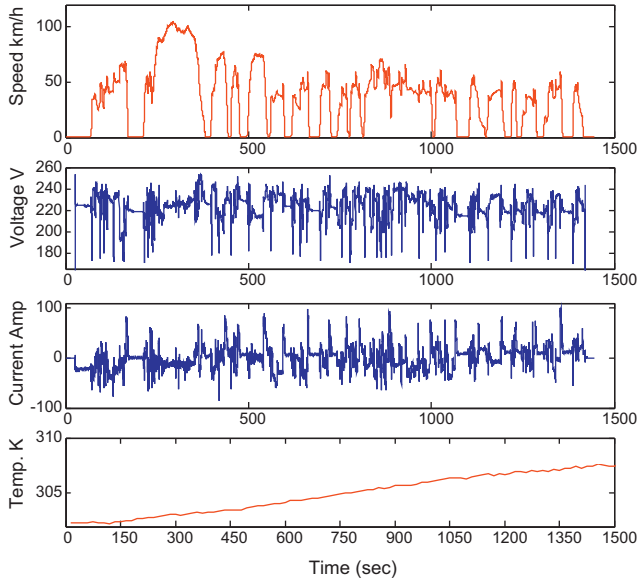

Fig. 7. Battery pack current, voltage and surface temperature during FUDS test.

simulate the forced convective heat transfer between the under hood components and the ambient air.

The solver is run for each drive cycle in order to simulate the heat transfer for the powertrain components. Each run time is set to 1 min step size with a tolerance slope of 5×10^{-7}, and the view factor accuracy is set to the maximum, i.e. it is selected to include 4608 rays that are cast from each element viewpoint. The relaxation factor is set to the adaptive mode, which allows the model to automatically check at each time step whether the relaxation factor needs to be adjusted in order to guarantee converged solution.

5. Results and discussion

5.1. Experimental results

The tests are designed to evaluate the battery pack thermal performance under controlled scenarios (i.e. load, speed, temperature, environment, current and voltage flows), in addition is aides in extracting the necessary boundary conditions for the FD simulation of the HEV thermal model.

The hybrid electric system is known to induce an electromagnetic interference with the signals collected during the tests, though several precautions were taken to reduce noise. The results obtained include: voltage, current, and actual surface temperature for the battery pack as recorded by infrared detector. Fig. 7 illustrates the results experienced during the FUDS drive cycle, showing that the pack is subject to an intensive charge/discharge cyclic loading. Though the signals encountered show some noise, it is still possible to notice the effect of the hybrid control system which is trying to maintain a certain limit of the pack voltage according to a predefined range. The surface temperature of the battery pack increases from 301 K to 307 K during the FUDS test.

On the other hand, artificial driving schedule demonstrates the steady state behavior of the hybrid control system as illustrated in Fig. 8. The test results show the pack surface temperature and the current flow at different vehicle speed intervals. The battery pack were discharged during the first portion of the first speed interval, i.e. 30 mph, meanwhile the system was recharging the pack for the rest of the ADC test.

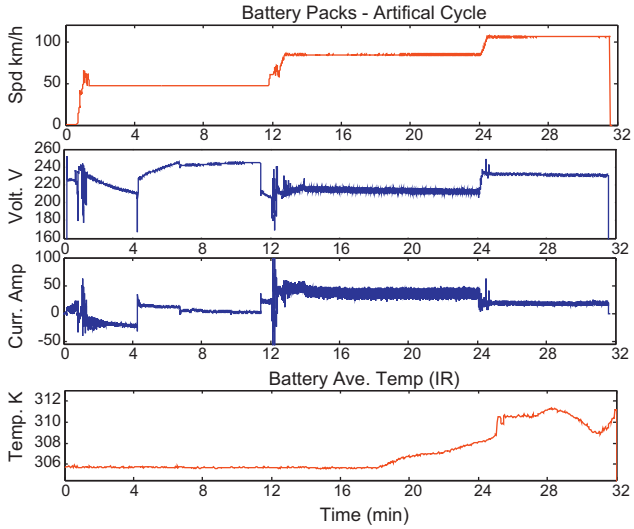

Fig. 8. Battery pack current, voltage and surface temperature during ADC test.

5.2. Simulation results

Subsequent to a successful acquisition of the boundary conditions with the aid of the available information from the test, the model was run for each of the driving cycles applied in the test (FHDS, FUDS and ADC), while the time duration for invoking the thermal solution was set according to the time extent of the drive cycle being simulated with 1 min time step size.

Under the transient and steady state current loads, the pack thermal behavior was monitored by selecting three battery cells at three different locations within the pack (one cell in the middle, and at the front and back of the battery pack). Fig. 13 illustrates a comparison of the temperature for the selected cells as recorded by the pre-existing OEM thermocouples (provided by the OBD) and the average surface temperature as obtained by the infrared detector; in contrast with average surface temperature for the same cells as predicted by the model during the artificial driving schedule (ADC). It should be noticed that the IR detector registers lower surface temperature for the pack, because it captures the temperature at the surface, while the thermocouples detect the temperature close to the core of the cells of the pack. Moreover, there is a lag

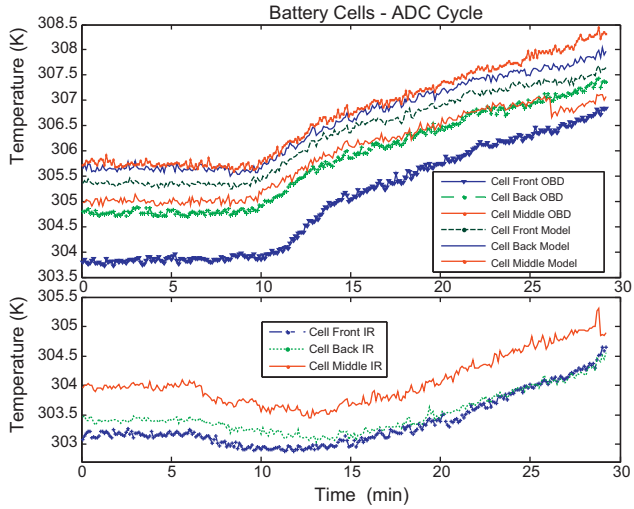

Fig. 9. Selected battery cell core and surface temperature as obtained by the IR detector and preexisted thermocouples in contrast with simulation results.

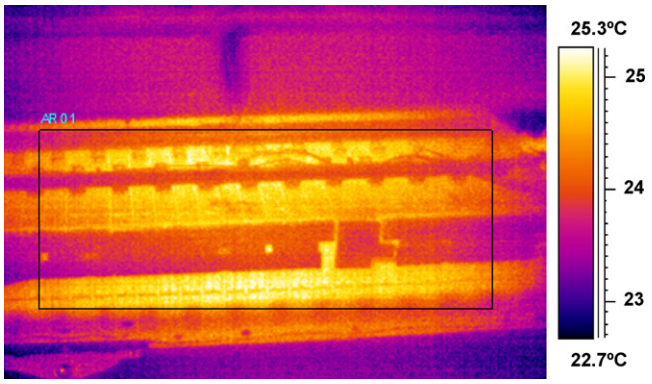

Fig. 10. Thermal image for the battery pack.

effect because the heat generated due to electrochemical activity requires some time to propagate/conduct to the cell surface. In addition to the excessive cooling air that flows over the exposed dismantled battery pack surface. It has been noticed that the model is slightly over predicting the surface temperature for the packs. It must be highlighted that the model computes the heat transfer for the powertrain under ideal conditions; in other words, the pack were packaged according to the standards of actual vehicle (materials properties, layers, etc.) for the enclosures, carpet, rear seat, were defined accurately, thus; the model will account for the heat exchanges between the pack and the surroundings, on the other hand, we the packs' enclosures and carpet were dismantled in order to allow for battery packs surface temperature measurements, hence; the cooling air from the chassis Dyno led to more heat to be dissipated away from the packs surface (Fig. 9).

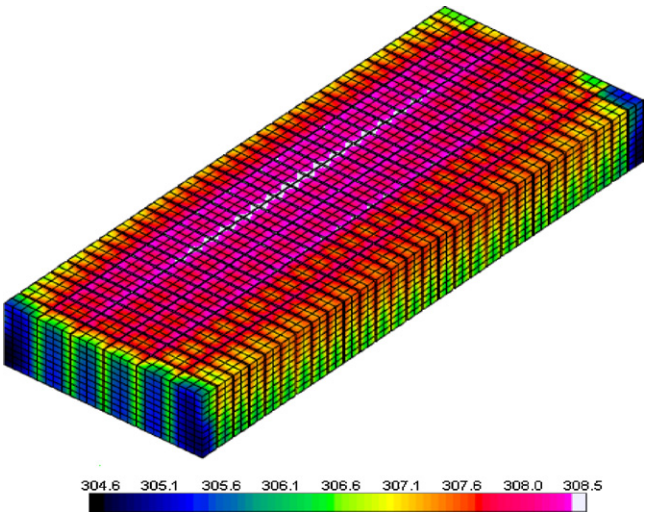

Fig. 11. Pack temperature maps at the end of the FUDS driving.

Fig. 10 shows a 2D thermal image obtained with the A40M Flir thermal camera illustrating the temperature profile across the battery pack at the end of the FHDS test. The cells at the middle region of the pack have the highest temperature in comparison to the cells at the border of the pack.

Fig. 11 illustrates the heat flux through the pack, at the end of the FUDS driving test as predicted by the model. The proposed 3D thermal model is able to predict the battery pack thermal performance as shown in Fig. 11. Also, Fig. 12 displays the battery cell

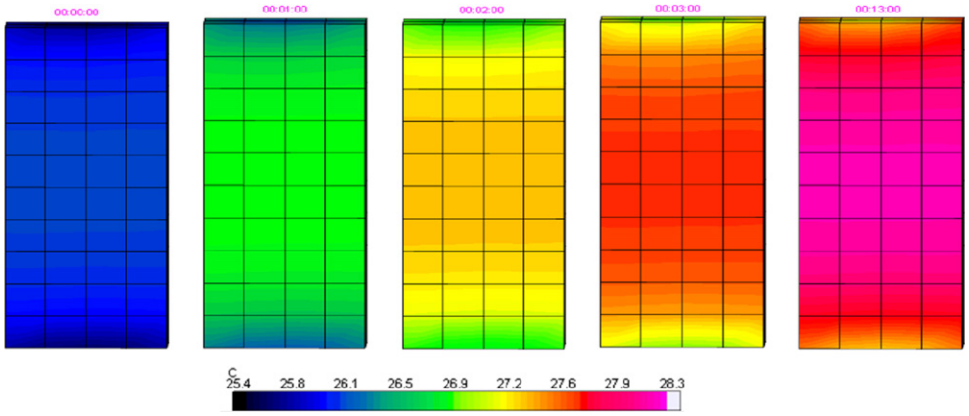

Fig. 12. Heat distribution and surface temperature for battery cell at minutes (0, 1, 3, and 13) under the FUDS driving test schedule.

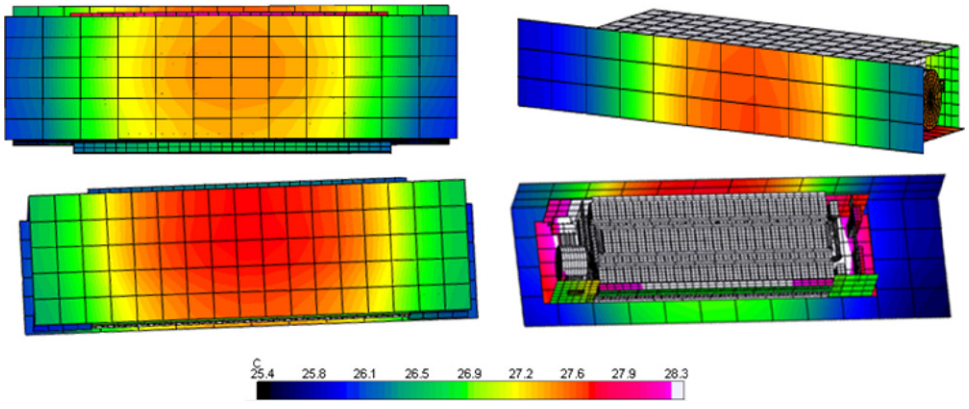

Fig. 13. Sample of thermal state for the battery pack enclosure after 10 min from ADC driving test.

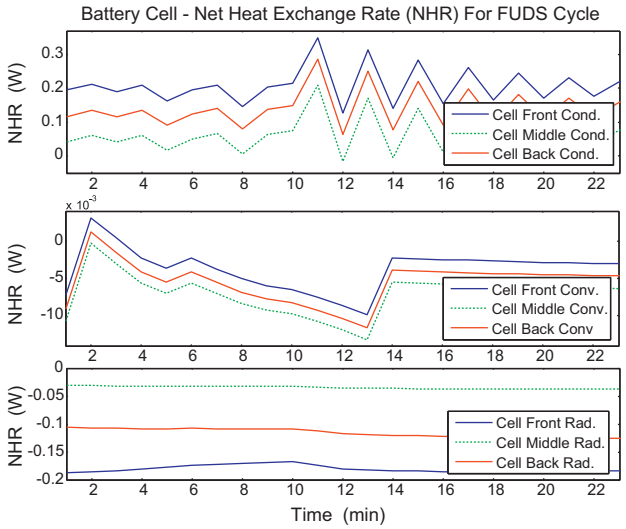

Fig. 14. Illustrates the net heat exchange rate by conduction, convection and radiation for the three pre-selected cells from the battery pack.

heat distribution and surface temperatures at minutes 0, 1, 3, 13 under the FUDS driving test schedule. Such illustration of the heat distribution allows for a constructive evaluation of the thermal loads under virtual conditions, which can then be used to assist the designer to develop an efficient Battery Thermal Management System (BTMS). In addition, such model can assist the designer in optimizing the packaging configurations and the utilization strategies for the pack under any packaging constraints at an early stage of the design process. Fig. 13 illustrates a sample of thermal state for the battery pack enclosure after 10 min during ADC driving test. This information can be used for an early prediction of the consequences of manipulating all possible packaging configurations for the pack under the constraints of limited space (compactness) and light-weight metrics.

Additionally, the model is capable of predicting the net heat exchange rates for geometrical parts and of simulating the heat transfer into/out of the different modules. Fig. 14 shows the net heat exchange rate for the three pre-selected cells from the battery pack. Conductive, convective and radiative heat exchange rates for three cells at different location in the pack are shown in Fig. 14. These results can also be used to devise new thermal control strategies in order to manipulate the BTMS and applying new cooling schemes for optimum operation of the pack under different loading patterns and environmental conditions. This is in addition to devising new material replacement [26–28] for the battery cell casing in a way to improve the thermal performance of the pack.

6. Conclusions

The presented work discusses the development of a comprehensive 3D thermal model for a power-split hybrid powertrain, including battery modules and power electronics. The model is constructed and validated for on-board hybrid system running under different standard and artificial driving cycles. The 3D thermal model was developed using a finite differencing algorithm complemented with experimentally extracted boundary conditions, which included; voltage, electric current, SOC, and the full-field and discrete temperature profiles. The proposed model predicts the spatial and temporal temperature profiles of the powertrain in agreement with the experimental data as provided by the vehicle control system.

The results show that the model is capable of predicting the thermal performance of the hybrid power train modules under controlled scenarios (load, speed, temperature, and environmental conditions). Furthermore, a cell based analysis is conducted to analyze the incident heat exchange rates by conduction, convection and radiation.

References

[1] EV, PHEV and EV Architectures, ECEN 2060 Class notes, spring 2008, http://www.ecee.colorado.edu/~ecen2060/materials/lecture/HEV_architectures.pdf.
[2] Application series from Fluent. 2003, Under Hood Thermal management, Fluent Inco, EX201, "http://www.fluent.com/".
[3] J. Popovic, J. Ferreira, IEEE Transactions on Power Electronics 20 (2005) 550–557.
[4] V.P.M. Govindasamy, Thermal modeling and imaging of as-built automotive parts, Thesis, University of Tennessee, Knoxville, 2004.
[5] A.F. Koschan, P. Govindasamy, S. Sreenivas, SAE 2006-01-1167.
[6] A.A. Pesaran, G.H. Kim, M. Keyser, EVS-24 International Battery, Hybrid and Fuel Cell Electric Vehicle Symposium Stavanger, Norway, May, 2009.
[7] A.A. Pesaran, Journal of Power Sources 110 (2002) 377–382.
[8] Toyota Prius Battery Packs Specification, 2010 "http://www.toyotaprius-battery.com/" last retrieved 2010.
[9] A. Moawad, G. Singh, S. Hagspiel, Proceedings of the 24th International Electric Vehicle Symposium and Exposition (EVS-24) (2009) 13–16.
[10] W. Hung, H. Tong, Lee S C., Transportation Research Part D: Transport and Environment 12 (2007) 115–128.
[11] M. Montazeri-Gh, M. Naghizadeh, Proceedings of 15th European Simulation Symposium, Delft, Netherlands, October, 2003.
[12] National Instrument user manual, National instrument LabVIEW full development (2010). Available from www.ni.com.
[13] Thermo-Vision A40M Researchers, 2010, FLIR SYSTEMS user manual 2010. Compact temperature measurements IR camera for research and development.
[14] M.Ö. Korukçu, M. Kilic, International Communications in Heat and Mass Transfer 36 (2009) 872–877.
[19] B.Y. Liaw, M. Dubarry, Journal of Power Sources 174 (2007) 76–88.
[20] Q. Wang, H. Huo, K. He, Transportation Research Part D: Transport and Environment 13 (2008) 289–297.
[21] P. Haan, M. Keller, BUWAL-Bericht SRU 255 (2001).
[22] Environmental Protection Agency, United States Of America, website "http://www.epa.com/" "Testing and Measurement Emissions" last retrieved Oct. 2010.
[23] T. Schwenn, Developer of Advanced Thermal Analysis and Infrared Signature Software, RadTherm Training, 2008.
[24] K. Johnson, A. Curran, D. Less, Proceedings of Ninth Annual Ground Target Modeling and Validation Conference, Houghton, MI, 1998.
[25] A.R. Curran, K.R. Johnson, E.A. Marttila, SAE International Congress & Exposition (1995), Paper No. 950615, Detroit, MI.
[26] R.R. Valisetty, R.R. Namburu, G. Petit, Parallel MuSES for Infrared Signature Modeling of US Army Vehicles and Targets, Army Research Laboratory, 2004, ARL-TR-328.
[27] K.R. Johns, B.S. Wood, P.L. Rynes, SAE International Congress & Exposition (1995), Paper No. 951012, Detroit, MI.
[28] M. Grujicic, V. Sellappan, M. Omar, Journal of Materials Processing Technology 197 (2008) 363–373.